Fabrication and characterization of B/Sn-doped ZnO nanoparticles via mechanochemical method for photocatalytic degradation of rhodamine B

Abrar Zadeed Ahmed, Md. Moinul Islam, Mohammed Monjur ul Islam, Shah Md. Masum, Rafiqul Islam & Md. Ashraful Islam Molla

To cite this article: Abrar Zadeed Ahmed, Md. Moinul Islam, Mohammed Monjur ul Islam, Shah Md. Masum, Rafiqul Islam & Md. Ashraful Islam Molla (2021) Fabrication and characterization of B/Sn-doped ZnO nanoparticles via mechanochemical method for photocatalytic degradation of rhodamine B, Inorganic and Nano-Metal Chemistry, 51:10, 1369-1378, DOI: 10.1080/24701556.2020.1835976

Fabrication and characterization of B/Sn-doped ZnO nanoparticles via mechanochemical method for photocatalytic degradation of rhodamine B

Abrar Zadeed Ahmed[a], Md. Moinul Islam[a], Mohammed Monjur ul Islam[b], Shah Md. Masum[a], Rafiqul Islam[a], and Md. Ashraful Islam Molla[a]

[a]Department of Applied Chemistry & Chemical Engineering, Faculty of Engineering & Technology, University of Dhaka, Dhaka, Bangladesh; [b]Institute of Functional Interfaces, Karlsruhe Institute of Technology, Eggenstein-Leopoldshafen, Germany

ABSTRACT

Undoped and B/Sn-doped ZnO nanoparticles are successfully produced by a simple mechanochemical method, and are characterized by XRD, FTIR, EDX, SEM, XPS and BET techniques. The XRD studies reveal that the prepared nanoparticles possess the hexagonal wurtzite structure of ZnO. The presence of various functional groups (–OH, –CH, Zn–O) are observed by FTIR. It is clear from EDX analysis that B, Sn, Zn and O elements are present in the nanoparticles. SEM images confirm the relatively smooth surface of B/Sn-doped ZnO nanoparticles. XPS results indicate that B and Sn are successfully doped into ZnO matrix. The photocatalytic performances of undoped and B/Sn-doped ZnO nanoparticles are investigated for the degradation of aqueous solution of Rhodamine B (RhB) dye in natural sunlight irradiation. The photocatalytic degradation of RhB dye in 1 h with B/Sn-doped ZnO nanoparticle is about 70.2%, which is significantly enhanced compared with the undoped ZnO (51.8%).

KEYWORDS

B/Sn doped ZnO; nanoparticles; photocatalytic degradation; mechanochemical method; rhodamine B

Introduction

Recently, semiconductor based photocatalytic degradation have attracted great attention as highly efficient green technology for the removal of organic pollutants from water.[1] ZnO is an n-type semiconductor which is well-known for its beneficial properties, such as large exciton energy (60 meV), wide direct band gap (3.27 eV), high optical gain (25 °C), high saturation velocity, piezoelectricity, pyroelectricity, nontoxicity, biocompatibility, good stability and low-cost synthesis.[2,3] ZnO nanomaterials have been extensively studied in various fields like photocatalysis, chemical sensors and solar cells.[4] Moreover, ZnO has been reported as a suitable photocatalyst to treat water containing several dye pollutants and solving environmental pollution problems.[5,6] However, the undoped ZnO exhibits low photocatalytic efficiency due to inadequate utilization of sunlight, rapid recombination of charge carriers and thus affect the catalysis rate of toxic dye degradation.[7,8] Hence, to harvest more sunlight for photocatalysis, it is necessary to reduce the band gap of the ZnO. Doping with nonmetals and/or metals can be considered as a feasible approach to improve its utilization of sunlight, charge separation efficiency and photostability of the catalyst.[9,10]

Different techniques have been employed for the synthesis of doped ZnO nanomaterials such as co-precipitation method,[11] sol-gel method,[12] combustion method,[6] hydrothermal method[13] and thermal decomposition method.[14] Doped ZnO has a significant role in a lot of applications, namely- light emitting diodes, UV lasers, solar cells, micro-electro-mechanical systems, transparent conducting electrodes, gas sensors and photocatalysts.[15–19] An assortment of metal dopants such as Ag, Au, Ce, Fe, Nb, Pd, V and many others are widely used as doping agents in ZnO.[20,21] Tin (Sn) is extensively used with ZnO owing to its photocatalytic activity by lowering the band gap, electron-hole pair generation, reduced recombination of photo induced charge carriers, and facilitating strength and improved morphology.[22] Unlike metal dopants, presently nonmetals like B, C, F, N, S etc. are being used to minimize electron hole recombination, improve grain size, increase surface area and so on.[23] Among them, B doping has attracted great consideration due to its atomic size and electronic structure.[24] Ahmad et al.[25] have synthesized B-doped ZnO nanostructures via the sol-gel method and summarized the optical and structural properties. Dindar et al.[26] have fabricated B-doped ZnO nanoparticles and studied the photocatalytic removal of rhodamine B dye under simulated sunlight. While Verma et al.[27] have employed combustion method to synthesize Sn-doped ZnO nanoparticles and reported the photocatalytic dye degradation. Siva et al.[28] have prepared Sn-doped ZnO nanoparticles through a chemical precipitation method and evaluated the photocatalytic activity. Priyadharsan et al.[29] have synthesized Sn-doped ZnO/rGO nanostructures using hydrothermal technique and investigated the structural and optical properties. However, to the best of our knowledge,

the synthesis of B/Sn-doped ZnO nanoparticles via the simple mechanochemical combustion method has not been reported.

Presently, undoped and B/Sn-doped ZnO nanoparticles are prepared by mechanochemical combustion method and subsequently characterized by XRD, SEM, EDX, FTIR, BET and XPS. The structural properties and the effects of B/Sn-doping in ZnO have been studied. The photocatalytic activities of undoped and B/Sn-doped ZnO nanoparticles are also investigated.

Experimental details

Chemicals

The following analytical grade reagents were used in the synthesis of the nanoparticle samples- zinc acetate dihydrate ($Zn(CH_3COO)_2{\cdot}2H_2O$), oxalic acid dihydrate ($(COOH)_2{\cdot}2H_2O$), boric acid (H_3BO_3) and tin chloride pentahydrate ($SnCl_4{\cdot}5H_2O$). All of the reagents were obtained from Merck (Germany). The reagents were not further purified. Deionized water was used for the preparation of solutions.

Synthesis method

Undoped and doped ZnO nanoparticles were synthesized by mechanochemical technique with controlled combustion method (Figure 1). At first, zinc acetate dihydrate (2.195 g) and oxalic acid dihydrate (2.521 g) were mixed and ground in an agate mortar for 10 minutes in order to obtain a paste of zinc oxalate dihydrate and acetic acid. The presence of acetic acid was confirmed by its typical smell. The loss of acetic acid in the form of fumes acted as a driving force for the reaction. Then, for the doped ones, boric acid and tin

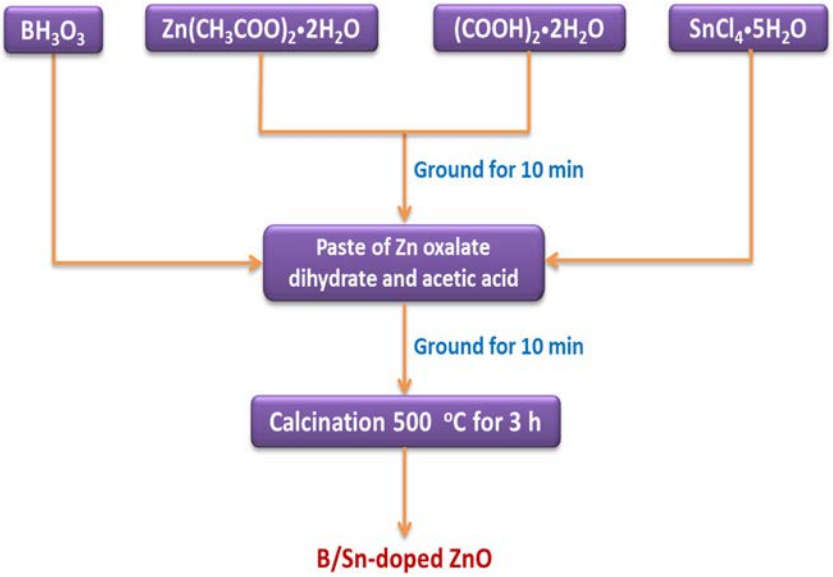

Figure 1. Synthesis of 3%B7%Sn/ZnO nanoparticles by mechanochemical combustion method.

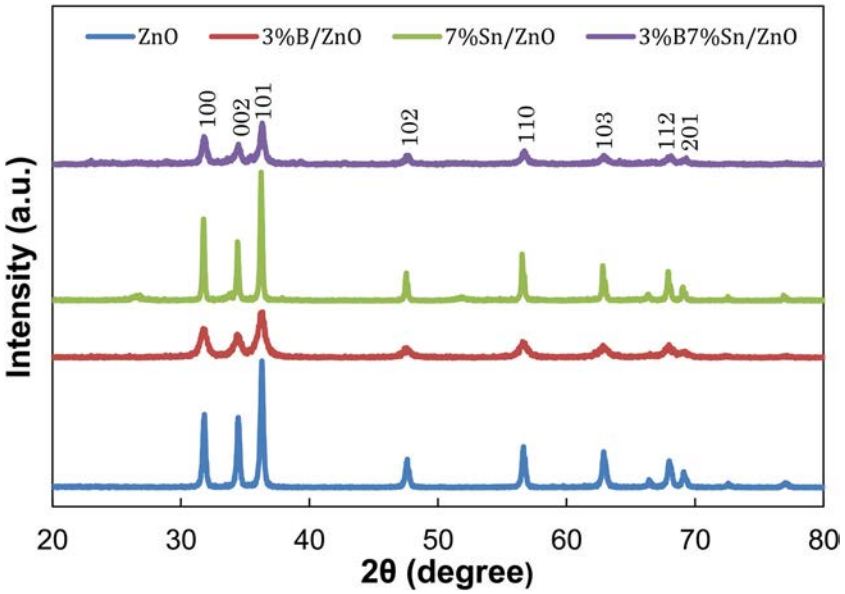

Figure 2. XRD patterns of ZnO, 3%B/ZnO, 7%Sn/ZnO and 3%B7%Sn/ZnO nanoparticles.

chloride pentahydrate as the sources for B and Sn respectively, were added to the paste and the grinding process was continued for a further 10 minutes to obtain the precursor. The undoped and doped ZnO crystallites were obtained by calcination of the precursors at a temperature of 500 °C for 3 hours under atmospheric conditions.[30]

Characterization

The diffraction patterns of the as-synthesized samples were collected using powder X-ray diffractometer (XRD, Ultima IV, Rigaku Corporation, Akishima, Japan) employing Cu Kα radiation ($\lambda = 0.15406$ nm, 40 KV, 1.64 mA) in 2θ angle range from 10° to 80°. A scanning electron microscope (SEM, TESCAN VEGA3, Brno, Czech Republic) equipped with an EDX system was used to record the morphologies and elemental analysis of undoped and doped ZnO. The chemical structures of the as-synthesized nanoparticles were studied using Fourier transformed infrared (FT-IR) spectrophotometer (IR Prestige-21, SHIMADZU, Japan) while the specific surface areas of those were determined by three points BET method with N_2 adsorption-desorption isotherms (Autosorb-1, Quantachrome Instruments, Florida, USA). X-ray photoelectron spectroscopy (XPS) measurements were carried out with IR/XPS-UHV system (Prevac) equipped with a VG Scienta R4000 electron energy analyzer using Al Kα (non-monochromatic, 1486.68 eV) radiation (CasaXPS database, v2.3.16, Rogów, Poland).

Photocatalytic activity evaluation

The photocatalytic activities of undoped and doped ZnO nanoparticles were examined by the degradation of RhB under sunlight irradiation at ambient temperature. Typically, 30 mL of RhB (10 mg/L) solution and 20 mg of synthesized photocatalyst was added to a 100 mL beaker. Experiments were conducted under similar conditions on a sunny day between 11:00 and 14:00. To equilibrate the suspension, a magnetic stirrer was used in the dark for 30 min. Then, the suspensions in the beakers were kept in sunlight for different time intervals. About 3 mL RhB solution was withdrawn and separated with an Advantec membrane filter 0.45 μm. The RhB concentration was calculated using a UV–visible spectrometry (UV-1700 Pharma Spec, SHIMADZU, Kyoto, Japan). The relative RhB concentration (C/C_0) was determined at the relative absorbance (A/A_0) of $\lambda = 549$ nm, according to the Beer–Lambert law, where A_0 and A were the absorbance of aqueous RhB at a starting time (t_0) of photodegradation and at any time t, respectively.

Results and discussion

XRD study

Figure 2 displays the XRD patterns of undoped and doped ZnO nanoparticles. The XRD spectra show distinct peaks at the specified positions of 31.76°, 34.46°, 36.32° and 56.64°,

Table 1. Summary of physical parameters.

Nanoparticles	2θ for (101)	Crystalline size (nm)	Lattice parameters (Å)		Volume (Å^3)
			a, d_{hkl} (101)	c, d_{hkl} (002)	
ZnO	36.30	27.87	3.237	5.245	47.61
3%B/ZnO	36.32	15.48	3.242	5.204	47.39
7%Sn/ZnO	36.24	41.94	3.250	5.209	47.66
3%B7%Sn/ZnO	36.32	23.22	3.242	5.206	47.40

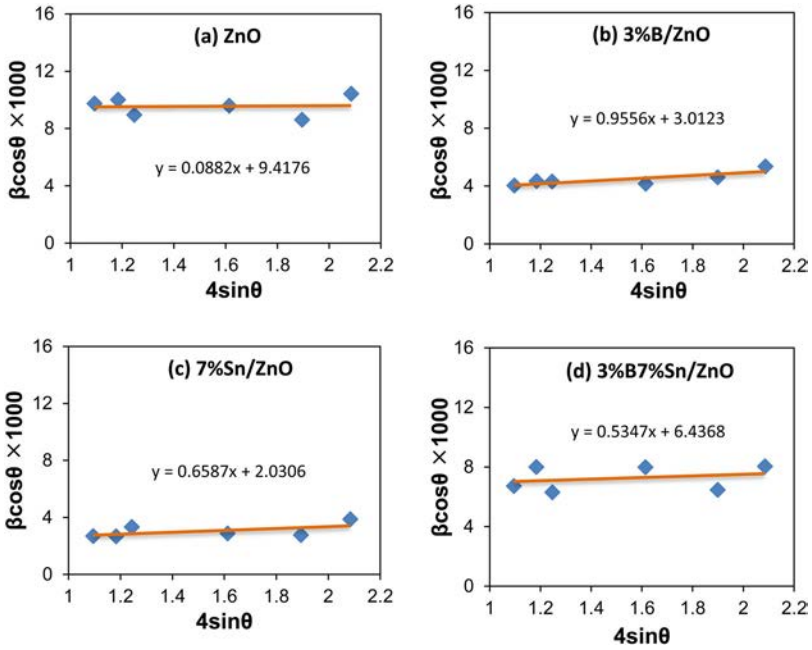

Figure 3. Williamson Hall plots of (a) ZnO, (b) 3%B/ZnO, (c) 7%Sn/ZnO and (d) 3%B7%Sn/ZnO nanoparticles.

which are in good agreement with the standard ZnO (JCPDS no.36–1451) and indexed as the hexagonal wurtzite structure of ZnO.[31] All nanoparticles of B-, Sn- and B/Sn-doped ZnO show strong peak of (101) and the intensity of the peak decreases with adding of B and B/Sn in ZnO.[32] The particle size of the oxides has been obtained from the full width at half maximum (FWHM) of the most intense peaks of the respective crystals using the Debye–Scherrer's equation:

$$D = \frac{k\lambda}{\beta \cos\theta} \tag{1}$$

where D is the average crystallite size, λ is the X–ray wavelength, θ is the Bragg diffraction angle, and β is the full width at half–maximum. The crystal size of B- and B/Sn-doped ZnO are smaller compared with those of the undoped ZnO (Table 1). The lattice parameters for hexagonal ZnO nanoparticles are estimated from the equation:

$$\frac{1}{d^2} = \frac{4}{3}\left(\frac{h^2 + hk + k^2}{a^2}\right) + \frac{l^2}{c^2} \tag{2}$$

where a and c are the lattice parameters and h, k and l are the Miller indices and d_{hkl} is the interplaner spacing for the plane (h k l). This interplaner spacing has been calculated from Bragg's law:

$$2d \sin\theta = n\lambda \tag{3}$$

The volume (V) of the unit cell for hexagonal system and the number of unit cells (n) in the particle can be calculated from the following equations:

$$V = 0.866 \times a^2 \times c \tag{4}$$

The strains of doped ZnO nanoparticles have been estimated and compared using the Williamson – Hall (W–H) equation[33]:

$$\beta \cos\theta = \frac{k\lambda}{D} + 4\varepsilon \sin\theta \tag{5}$$

where ε is the strain associated with the doped ZnO nanoparticles. Equation (5) illustrates a straight line between 4 sin θ (X–axis) and β cos θ (Y–axis). The slope of line gives the strain (ε) and intercept (k/D) of this line on Y–axis provides the grain size (D). The crystal strains of undoped and doped ZnO are obtained from the slope (η) of the W – H plot, as shown in Figure 3. Positive slopes of 0.00095, 0.00065 and 0.00053 are obtained in B-, Sn- and B/Sn-doped ZnO nanoparticles, respectively, describing the tensile strain

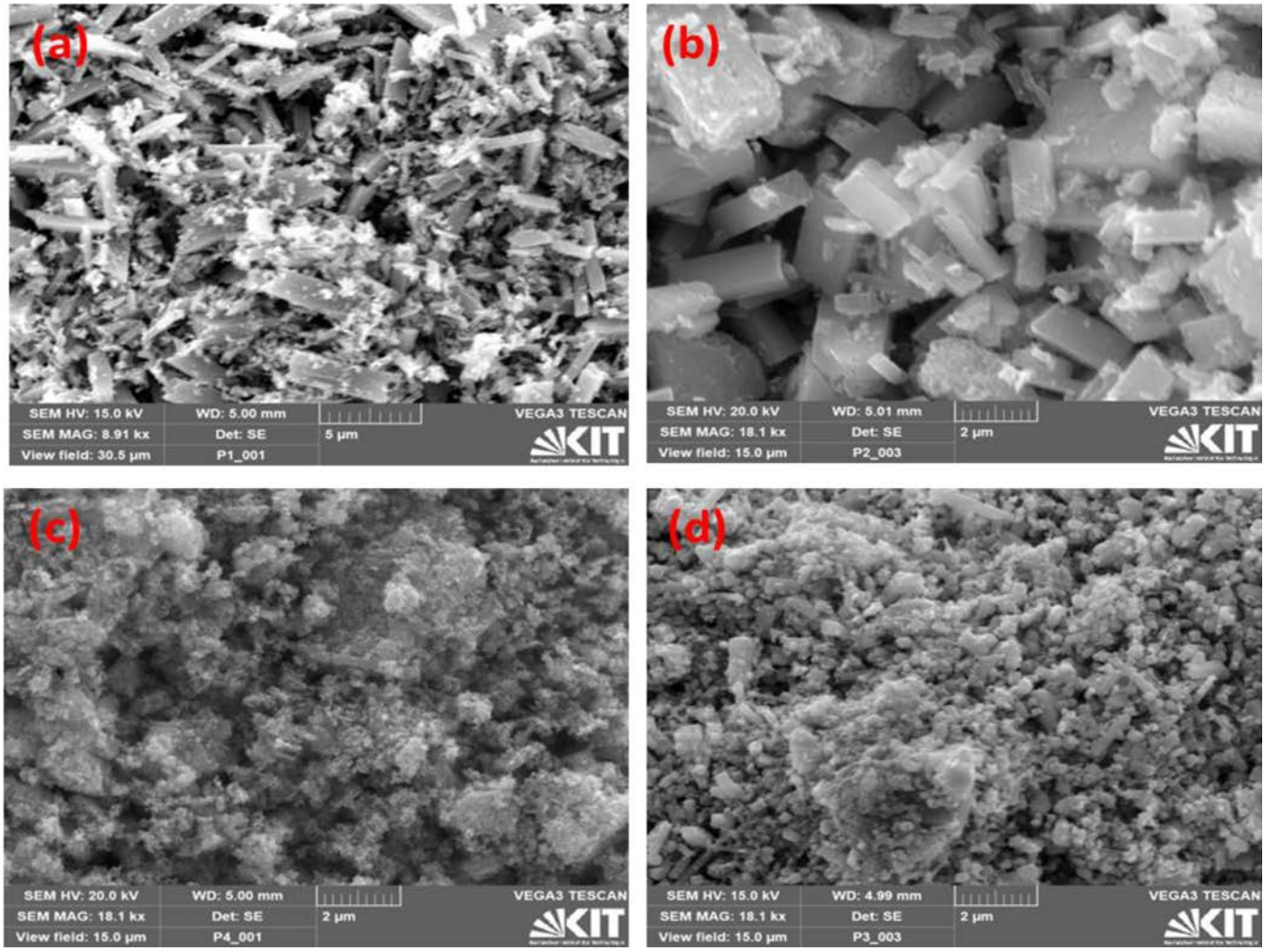

Figure 4. SEM images of (a) ZnO, (b) 3%B/ZnO, (c) 7%Sn/ZnO and (d) 3%B7%Sn/ZnO nanoparticles.

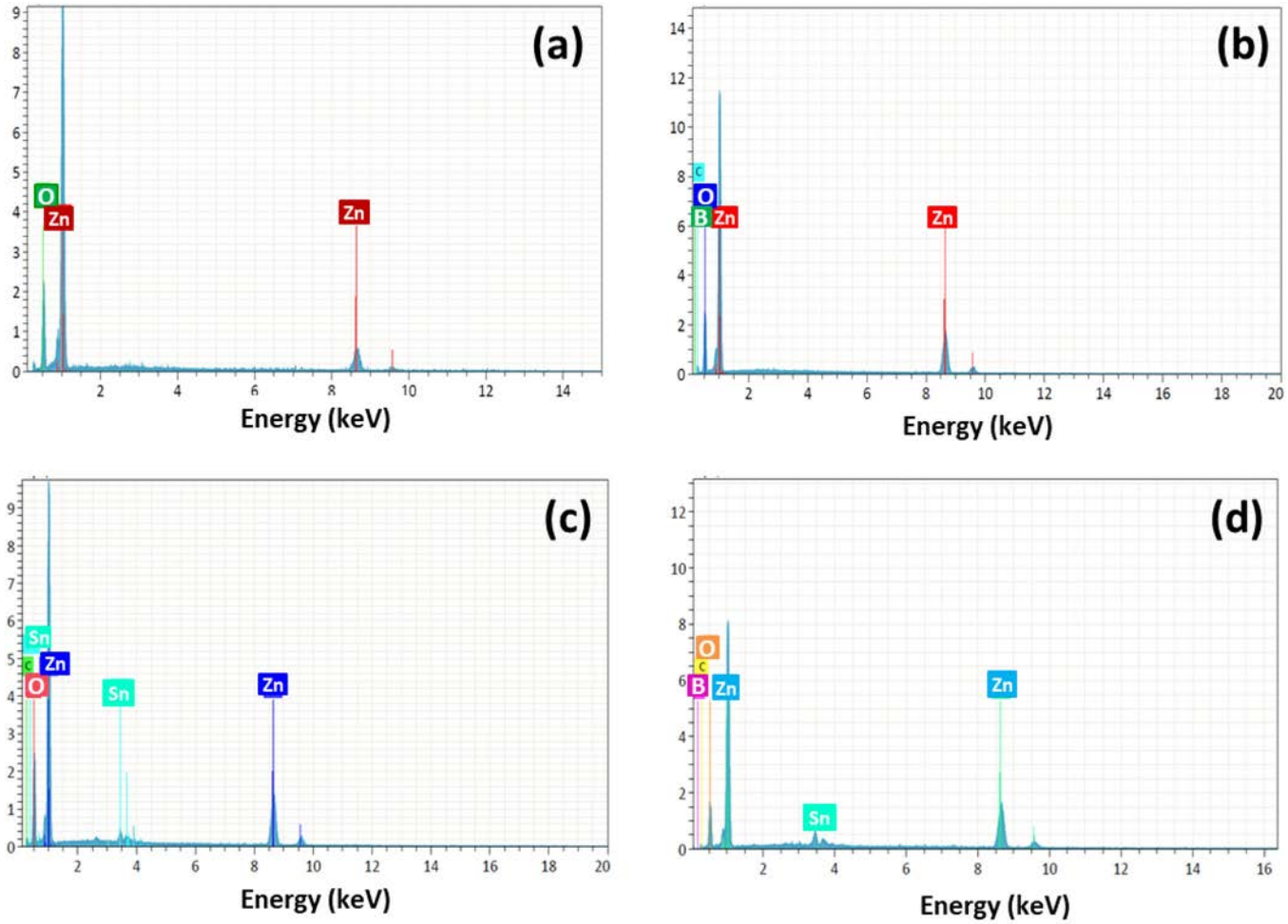

Figure 5. EDX pattern of (a) ZnO, (b) 3%B/ZnO, (c) 7%Sn/ZnO and (d) 3%B7%Sn/ZnO nanoparticles.

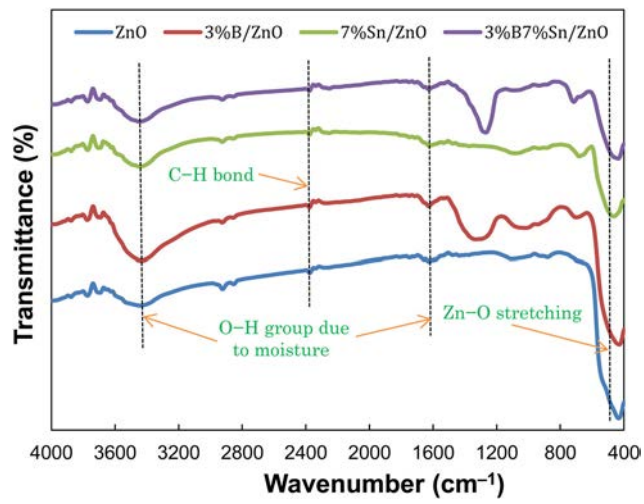

Figure 6. FTIR spectra of ZnO, 3%B/ZnO, 7%Sn/ZnO and 3%B7%Sn/ZnO nanoparticles.

for crystal ZnO. The lattice parameters and cell volume values have been calculated from the XRD data, as shown in Table 1. Consequently, the effects of B- and B/Sn-doping describe the following characteristics of: (i) XRD peaks broadening (ii) crystallinity degradation, (iii) crystallite size reduction, (iv) smaller particle size and (v) tensile strain.

SEM study

Figure 4 presents the surface morphologies of the undoped and doped ZnO nanomaterials evaluating by SEM. The synthesized undoped ZnO is heterogeneous in nature and distributed over the surface with the rod shape branches of building blocks shown in Figure 4(a). On the other hand, Figure 4(b) shows that the shape of the B-doped ZnO particles changed from rod-like to spheroid. As shown in SEM Figure 4(c), Sn-doped ZnO nanoparticles are spherical like structures and have high degree of agglomeration. After doping B and Sn, the surface of B/Sn-doped ZnO particles become relatively smooth as shown in Figure 4(d). The morphologies of B-, Sn- and B/Sn-doped ZnO nanoparticles are different from the undoped ZnO. The average size of the particles as observed by SEM is in the nanometer range, which is consistent with the XRD results.

EDX study

Figure 5 shows the EDX line-scanning results of undoped and doped ZnO nanoparticles. The EDX spectrum of undoped ZnO has sharp peaks of elemental Zn and O as shown in Figure 5(a). The EDX spectra of B-doped ZnO contain peaks corresponding to the elements of B, Zn and O (Figure 5b). In Figure 5(c), the EDX spectra of Sn-doped

ZnO show the strong signals of element Sn, Zn and O. The EDX spectra analysis of B/Sn-doped ZnO indicates the presence of all the four elements of B, Sn, Zn, and O (Figure 5(d)). EDX spectra confirm the formation of pure undoped and doped ZnO nanoparticles.

FTIR study

Figure 6 illustrates the FTIR results of undoped and doped ZnO nanoparticles. IR spectra demonstrate that the zinc oxide absorption band with stretching mode of Zn – O is between 400 cm ^{1} to 590 cm ^{1}, which corresponds to the hexagonal ZnO wurtzite crystal structure.[34] The fundamental mode of vibration near 3385 cm ^{1} and 1637 cm ^{1} corresponds to the asymmetric and symmetric stretching of H – O–H vibration. The very weak peak observed at 2370 cm ^{1} is attributed to the symmetric C – H bond vibrations which may be present due to the environmental conditions. The signal between 1600 and 700 cm ^{1} assigns to B – O stretching vibrations which indicates boron incorporation into ZnO.[35] The 3000–3650 cm ^{1} bands are due to the reversible dissociative absorption of hydrogen on Zn as well as O site.[36]

BET study

Figure 7 shows the N_2 adsorption/desorption curves of the undoped and doped ZnO nanomaterials. It is observed that the adsorption/desorption curves are of type IV which are exemplary for mesoporous materials based on the IUPAC classication.[37] The detailed physical characteristics of the undoped and doped ZnO nanoparticles are given in Table 2. The BET surface area and pore volume of undoped ZnO are of 8.4 m^2/g and 0.146 cm^3/g whereas the surface area of B-, Sn- and B/Sn-doped ZnO are 36.8 m^2/g, 17.7 m^2/g and 2.14 m^2/g with pore volume of 0.287 cm^3/g, 0.073 cm^3/g and 0.001 cm^3/g, respectively.

XPS study

The surface compositions and their corresponding valence state of the B/Sn-doped ZnO have been investigated with

Table 2. BET parameters of ZnO, 3%B/ZnO, 7%Sn/ZnO and 3%B7%Sn/ZnO nanoparticles.

Nanoparticles	BET surface area (m^2/g)	Pore volume (cm^3/g)
ZnO	8.45	0.146
3%B/ZnO	36.88	0.287
7%Sn/ZnO	7.70	0.073
3%B7%Sn/ZnO	2.14	0.001

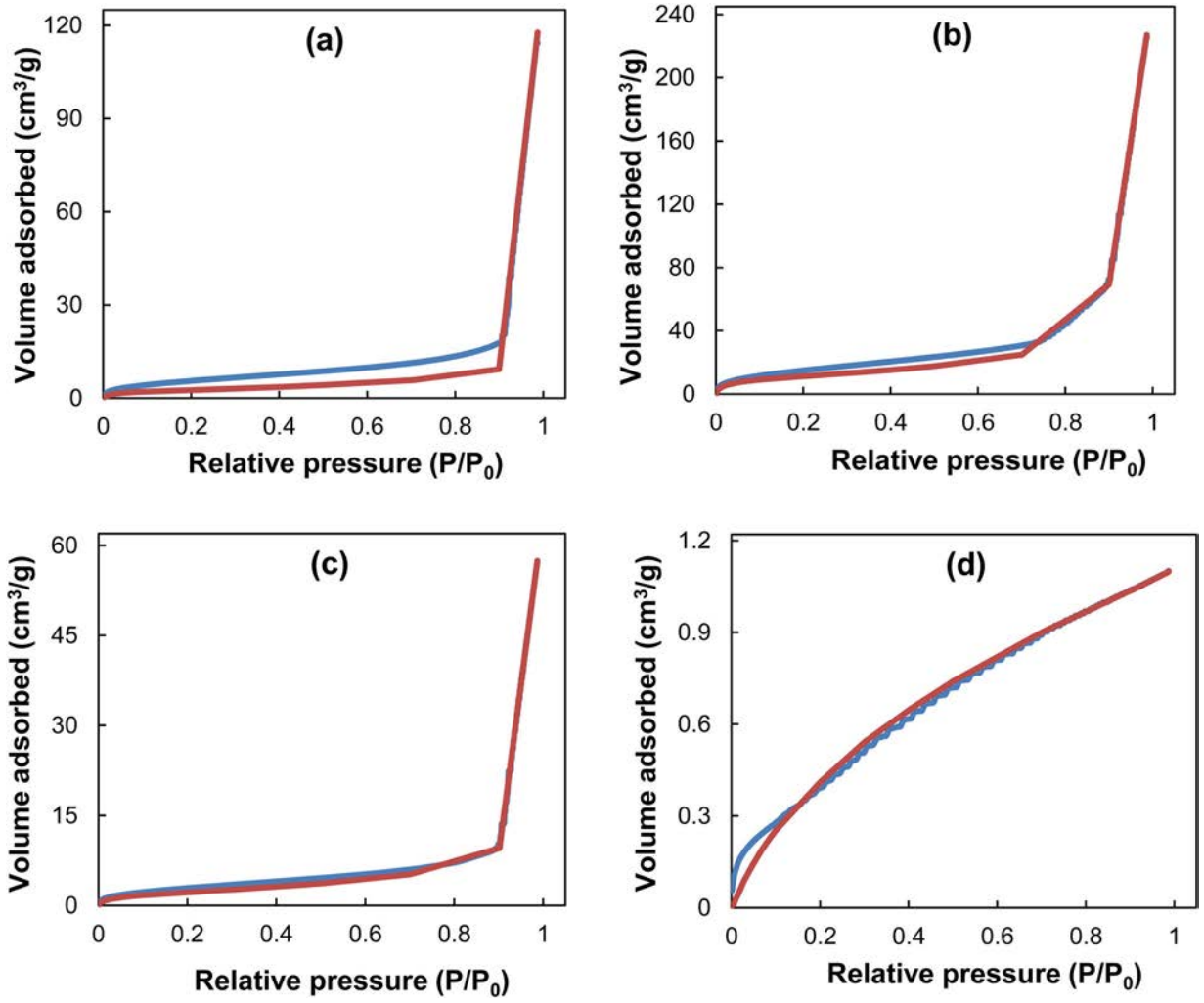

Figure 7. N_2 adsorption/desorption isotherms of (a) ZnO, (b) 3%B/ZnO, (c) 7%Sn/ZnO and (d) 3%B7%Sn/ZnO nanoparticles.

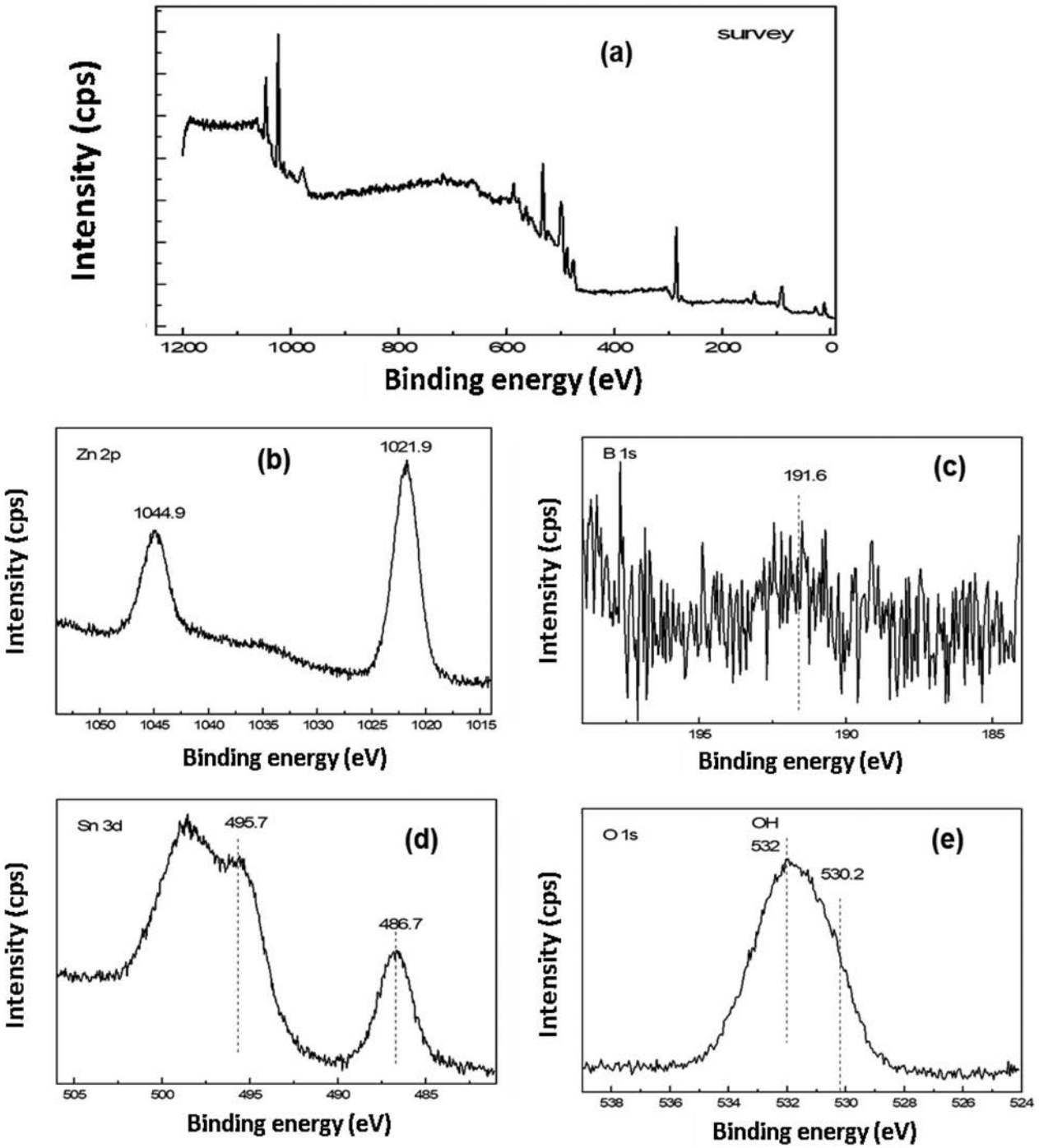

Figure 8. XPS spectrum of (a) 3%B7%Sn/ZnO nanoparticles, (b) Zn 2p, (c) B 1 s, (d) Sn 3d, and (e) O 1 s of acquired with Al Kα radiations.

XPS. Figure 8(a) exhibits the XPS full survey spectrum, from which the peaks of Zn, B, Sn, O and C elements can be observed clearly. The C element might be from hydrocarbons during the synthesis process. Therefore, the nanoparticles are composed of Zn, B, Sn and O only and these results are agreement with the XRD patterns. Figure 8(b) presents the high resolution spectra for Zn 2p. In Figure 8(b), the peaks centered at 1021.9 and 1044.9 eV are attributed to the Zn $2p_{3/2}$ and Zn $2p_{1/2}$ of Zn^{2+}.[30] The binding energy peak of B 1 s shown in the Figure 8(c) is located at 191.6 eV, indicate that the doping B atoms are in the trivalent state of B^{3+}.[38] The peaks appearing in Figure 8(d) are located at 486.7 and 495.7 eV, which are ascribed to the Sn $3d_{5/2}$ and Sn $3d_{3/2}$ of Sn^{4+}, respectively.[39] Figure 8(e) shows the spectrum of O 1 s which illustrates the chemical state of oxygen in the prepared nanomaterials. The peak appeared at 530.2 eV represents the metal bonded oxygen as Zn–O whereas the other located at 532 eV reveals the presence of hydroxyl groups on the surface of the nanoparticles.[40]

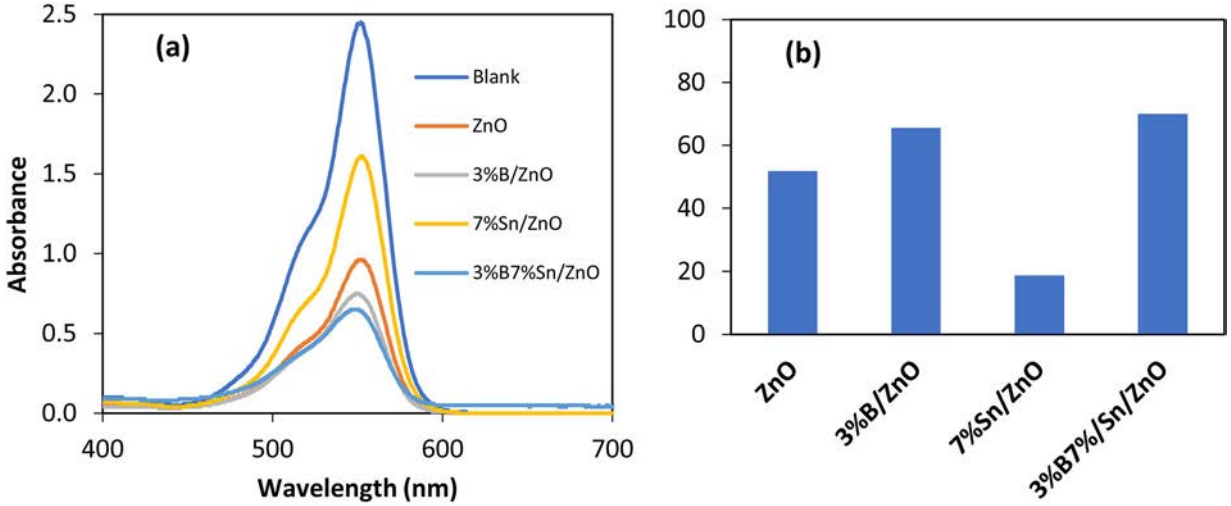

Figure 9. (a) UV visible spectral changes and (b) Photocatalytic degradation of RhB with undoped and B/Sn doped ZnO nanoparticles after 1 h sunlight irradiation.

Photocatalytic RhB dye degradation

Undoped and B/Sn-doped ZnO nanoparticles are used in the presence of sunlight for the photodegradation of RhB dye to evaluate the photocatalytic performance. The UV–visible absorption spectrum of RhB dye shows a peak at 549 nm (Figure 9(a)). The absorption intensities of the peaks decrease with undoped and doped ZnO, which confirms the progress of the photocatalytic degradation of the RhB dye. The effect of the dopants in the photodegradation of RhB is depicted in Figure 9(b). The degradation is greater with B-doped and B/Sn-doped ZnO, but Sn doped ZnO shows similar performance as undoped ZnO. With B-doped and B/Sn-doped ZnO the degradation percentage is 65.6% and 70.2% respectively but Sn-doped one shows similar performance as the undoped ZnO, about 51.8%. Thus, B/Sn-doped ZnO can enhance the degradation rate and improve the photocatalytic activity which is attributed to the doping effect of both B and Sn together in the nanoparticles.

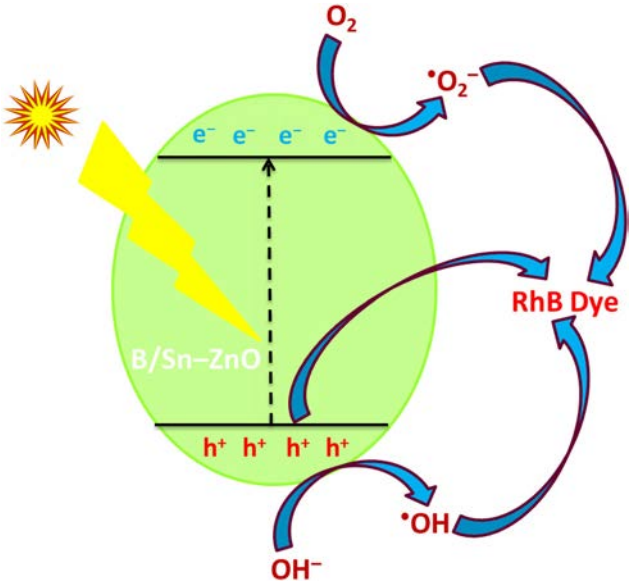

Figure 10. Photocatalytic RhB dye degradation mechanism by B/Sn doped ZnO with sunlight.

Plausible RhB dye degradation mechanism

The photocatalytic RhB dye degradation mechanism with B/Sn-doped ZnO photocatalyst is demonstrated in Figure 10. When sunlight is provided, RhB dye is degraded significantly by B/Sn-doped ZnO. Because, the photogenerated electrons (e) and holes (h^+) in doped ZnO become lighter and heavier compared with undoped ZnO. The combination of lighter e and heavier h^+ in doped ZnO is beneficial for the separation of photogenerated h^+/e pairs and improves its photocatalytic performance.[41] During sunlight irradiation to photocatalyst, B/Sn-doped ZnO can easily absorb light energy to create h^+/e pairs. Then, the photogenerated h^+ can degrade RhB dye directly or react with the water (H_2O) to produce $^{\bullet}OH$ radical.[9] The photoexcited e attack the dissolved oxygen (O_2) to produce $^{\bullet}O_2$ radical, which can degrade RhB dye.[9] Moreover, the e can interact with the H_2O continuously to generate $^{\bullet}OH$ radical, which is the strong oxidative agent in the photocatalytic reaction to degrade RhB dye into CO_2, H_2O and other degradation products.[42,43] Therefore, the plausible photocatalytic RhB dye degradation reactions by B/Sn-doped ZnO with sunlight can be summarized as follows.[44,45]

$$\text{Photocatalyst} + h\nu(\text{Sunlight}) \rightarrow e + h^+ \quad (6)$$

$$e + O_2 \rightarrow \bullet O_2 \quad (7)$$

$$^{\bullet}O_2 + H_2O \rightarrow {}^{\bullet}OH + OH + 1/2O_2 \quad (8)$$

$$h^+ + H_2O \rightarrow H^+ + \bullet OH \quad (9)$$

$$^{\bullet}O_2 + \text{RhB dye} \rightarrow \text{Degradation products} \quad (10)$$

$$h^+ + \text{RhB dye} \rightarrow \text{Degradation products} \quad (11)$$

$$^{\bullet}OH + \text{RhB dye} \rightarrow \text{Degradation products} \quad (12)$$

Conclusion

A facile one-step mechanochemical combustion method is used to synthesize a novel B/Sn-doped ZnO nanoparticle

photocatalyst. The material characteristics and photodegradation activities of the nanoparticle have been investigated. XRD measurement shows that the average crystallite sizes of undoped and B/Sn-doped ZnO are ~28 nm and ~23 nm, respectively. The FTIR spectra demonstrate the stretching mode of Zn − O in between 400 cm ^{1} to 590 cm ^{1}. The survey spectrum of B/Sn-doped ZnO exhibits the presence of B-1s, Sn-3d, Zn-2p and O-1s peaks. All the nanoparticles indicate typical type IV isotherm according to the IUPAC classification. The B/Sn-doped ZnO nanoparticles are found to exhibit better photocatalytic performance for RhB dye degradation in comparison with the undoped ZnO. Therefore, the photocatalytic degradation treatment of wastewater including dye pollutants by sunlight is an easy and simple technique, and cost-effective.

Acknowledgment

The authors are grateful to the Centre for Advanced Research in Sciences (CARS), University of Dhaka, Bangladesh for providing partial analytical support.

Disclosure statement

The authors declare that they do not have any conflicts of interest.

Funding

This research was funded by the Ministry of Science and Technology, Bangladesh (39.00.0000.09.06.90.18 19/311/EAS 10).

References

1. Kumar, S.; Sharma, V.; Bhattacharyya, K.; Krishnan, V. N Doped ZnO MoS_2 Binary Heterojunctions: Dual Role of 2D MoS_2 in the Enhancement of Photostability and Photocatalytic Activity under Visible Light Irradiation for Tetracycline Degradation. *Mater. Chem. Front.* **2017**, *1*, 1093 1106. DOI: 10.1039/C6QM00274A.
2. Vignesh, S.; Suganthi, S.; Sundar, J. K.; Raj, V.; Devi, P. R. I. Highly Efficient Visible Light Photocatalytic and Antibacterial Performance of PVP Capped Cd:Ag:ZnO Photocatalyst Nanocomposites. *Appl. Surf. Sci.* **2019**, *479*, 914 929. DOI: 10.1016/j.apsusc.2019.02.064.
3. Molla, M. A. I.; Furukawa, M.; Tateishi, I.; Katsumata, H.; Kaneco, S. Fabrication of Ag Doped ZnO by Mechanochemical Combustion Method and Their Application into Photocatalytic Famotidine Degradation. *J. Environ. Sci. Health Part A* **2019**, *54*, 914 923. DOI: 10.1080/10934529.2019.1608793.
4. Kumar, P.; Kumar, A.; Rizvi, M. A.; Moosvi, S. K.; Krishnan, V.; Duvenhage, M. M.; Roos, W. D.; Swart, H. C. Surface, Optical and Photocatalytic Properties of Rb Doped ZnO Nanoparticles. *Appl. Surf. Sci.* **2020**, *514*, 145930. DOI: 10.1016/j.apsusc.2020.145930.
5. Shanmugam, V.; Jeyaperumal, K. S. Investigations of Visible Light Driven Sn and Cu Doped ZnO Hybrid Nanoparticles for Photocatalytic Performance and Antibacterial Activity. *Appl. Surf. Sci.* **2018**, *449*, 617 630. DOI: 10.1016/j.apsusc.2017.11.167.
6. Sakib, A. A. M.; Masum, S. M.; Hoinkis, J.; Islam, R.; Molla, M. A. I. Synthesis of CuO/ZnO Nanocomposites and Their Application in Photodegradation of Toxic Textile Dye. *J. Compos. Sci.* **2019**, *3*, 91. DOI: 10.3390/jcs3030091.
7. Kumar, S.; Dhiman, A.; Sudhagar, P.; Krishnan, V. ZnO Graphene Quantum Dots Heterojunctions for Natural Sunlight Driven Photocatalytic Environmental Remediation. *Appl. Surf. Sci.* **2018**, *447*, 802 815. DOI: 10.1016/j.apsusc.2018.04.045.
8. Bhuvaneswari, K.; Vaitheeswari, V.; Palanisamy, G.; Maiyalagan, T.; Pazhanivel, T. Glutathione Capped Inverted Core Shell Quantum Dots as an Efficient Photocatalyst for Degradation of Organic Dyes. *Mater. Sci. Semicond. Process.* **2020**, *106*, 104760. DOI: 10.1016/j.mssp.2019.104760.
9. Kabir, R.; Saifullah, M. A. K.; Ahmed, A. Z.; Masum, S. M.; Molla, M. A. I. Synthesis of N Doped ZnO Nanocomposites for Sunlight Photocatalytic Degradation of Textile Dye Pollutants. *J. Compos. Sci.* **2020**, 4, 49.
10. Kumar, S.; Kumar, A.; Kumar, A.; Krishnan, V. Nanoscale Zinc Oxide Based Heterojunctions as Visible Light Active Photocatalysts for Hydrogen Energy and Environmental Remediation. *Catal. Rev.* **2020**, 4, 346 404. DOI: 10.3390/jcs4020049.
11. Zafar, M. N.; Dar, Q.; Nawaz, F.; Zafar, M. N.; Iqbal, M.; Nazar, M. F. Effective Adsorptive Removal of Azo Dyes over Spherical ZnO Nanoparticles. *J. Mater. Res. Technol.* **2019**, *8*, 713 725. DOI: 10.1016/j.jmrt.2018.06.002.
12. Hasnidawani, J. N.; Azlina, H. N.; Norita, H.; Bonnia, N. N.; Ratim, S.; Ali, E. S. Synthesis of ZnO Nanostructures Using Sol Gel Method. *Procedia Chem.* **2016**, *1*, 211 216.
13. Nava Núñez, M. Y.; Martínez de la Cruz, A. Nitric Oxide Removal by Action of ZnO Photocatalyst Hydrothermally Synthesized in Presence of EDTA. *Mater. Sci. Semicond. Process.* **2018**, *81*, 94 101. DOI: 10.1016/j.mssp.2018.03.012.
14. Kaur, J.; Bansal, S.; Singhal, S. Photocatalytic Degradation of Methyl Orange Using ZnO Nanopowders Synthesized via Thermal Decomposition of Oxalate Precursor Method. *Phys. B Condens. Matter* **2013**, *416*, 33 38. DOI: 10.1016/j.physb.2013.02.005.
15. Hjiri, M.; El Mir, L.; Leonardi, S. G.; Pistone, A.; Mavilia, L.; Neri, G. Al Doped ZnO for Highly Sensitive CO Gas Sensors. *Sens. Actuators B Chem.* **2014**, *196*, 413 420. DOI: 10.1016/j.snb.2014.01.068.
16. Mendoza Mendoza, E.; Nuñez Briones, A. G.; García Cerda, L. A.; Peralta Rodríguez, R. D.; Montes Luna, A. J. One Step Synthesis of ZnO and Ag/ZnO Heterostructures and Their Photocatalytic Activity. *Ceram. Int.* **2018**, *44*, 6176 6180. DOI: 10.1016/j.ceramint.2018.01.001.
17. Lahmer, M. A. The Effect of Doping with Rare Earth Elements (Sc, Y, and La) on the Stability, Structural, Electronic and Photocatalytic Properties of the O Terminated ZnO Surface; a First Principles Study. *Appl. Surf. Sci.* **2018**, *457*, 315 322. DOI: 10.1016/j.apsusc.2018.06.273.
18. Li, Y.; Gao, Z.; Qin, W.; Wen, Q.; Jun, M. Nano Size Related Piezoelectric Efficiency in a Large ZnO Thin Film, Potential for Selfpowered Medical Device Application. *Biochem. Anal. Biochem.* **2016**, *5*, 2161 1009.
19. Haq, B. U.; Ahmed, R.; Shaari, A.; Ali, N.; Al Douri, Y.; Reshak, A. Comparative Study of Fe Doped ZnO Based Diluted and Condensed Magnetic Semiconductors in Wurtzite and Zinc Blende Structures by First Principles Calculations. *Mater. Sci. Semicond. Process.* **2016**, *43*, 123 128. DOI: 10.1016/j.mssp.2015.12.010.
20. Qi, K.; Cheng, B.; Yu, J.; Ho, W. Review on the Improvement of the Photocatalytic and Antibacterial Activities of ZnO. *J. Alloys Compd.* **2017**, *727*, 792 820. DOI: 10.1016/j.jallcom.2017.08.142.
21. Mousavi, S. M.; Mahjoub, A. R.; Abazari, R. Facile Green Fabrication of Nanostructural Ni Doped ZnO Hollow Sphere as an Advanced Photocatalytic Material for Dye Degradation. *J. Mol. Liq.* **2017**, *242*, 512 519. DOI: 10.1016/j.molliq.2017.07.050.
22. Turkyilmaz, S. S.; Guy, N. M. Photocatalytic Efficiencies of Ni, Mn, Fe and Ag Doped ZnO Nanostructures Synthesized by Hydrothermal Method: The Synergistic/Antagonistic Effect between ZnO and Metals. *J. Photochem. Photobiol. A Chem.* **2017**, *341*, 39 50.

23. Wang, Y.; Huang, Y.; Ho, W.; Zhang, L.; Zou, Z.; Lee, S. Biomolecule Controlled Hydrothermal Synthesis of C N S Tridoped TiO_2 Nanocrystalline Photocatalysts for NO Removal under Simulated Solar Light Irradiation. *J. Hazard. Mater.* **2009**, *169*, 77 87. DOI: 10.1016/j.jhazmat.2009.03.071.
24. Kumar, S.; Maivizhikannan, V.; Drews, J.; Krishnan, V. Fabrication of Nanoheterostructures of Boron Doped ZnO MoS_2 with Enhanced Photostability and Photocatalytic Activity for Environmental Remediation Applications. *Vacuum* **2019**, *163*, 88 98. DOI: 10.1016/j.vacuum.2019.02.001.
25. Ahmad, A. A.; Alsaad, A. M.; Al Bataineh, Q. M.; Al Naafa, M. A. Optical and Structural Investigations of Dip Synthesized Boron Doped ZnO Seeded Platforms for ZnO Nanostructures. *Appl. Phys. A* **2018**, *124*, 458. DOI: 10.1007/s00339 018 1875 z.
26. Dindar, B.; Guler, A. C. Comparison of Facile Synthesized N Doped, B Doped and Undoped ZnO for the Photocatalytic Removal of Rhodamine B. *Environ. Nanotechnol. Monit. Manag.* **2018**, *10*, 457 466.
27. Verma, N.; Bhatia, S.; Bedi, R. K. Sn Doped ZnO Nanopetal Networks for Efficient Photocatalytic Degradation of Dye and Gas Sensing Applications. *Appl. Surf. Sci.* **2017**, *407*, 495 502.
28. Siva, N.; Sakthi, D.; Ragupathy, S.; Arun, V.; Kannadasan, N. Synthesis, Structural, Optical and Photocatalytic Behavior of Sn Doped ZnO Nanoparticles. *Mater. Sci. Eng. B* **2020**, *253*, e114497. DOI: 10.1016/j.mseb.2020.114497.
29. Priyadharsan, A.; Shanavas, S.; Vidya, C.; Sundar, J. K.; Acevedo, R.; Anbarasan, P. M. Structural and Optical Properties of Sn Doped ZnO rGO Nanostructures Using Hydrothermal Technique. Mater. Today: *Proc.* **2020**, *26*, 3522 3525. DOI: 10. 1016/j.matpr.2019.05.440.
30. Molla, M. A. I.; Furukawa, M.; Tateishi, I.; Katsumata, H.; Kaneco, S. Studies of Effects of Calcination Temperature on the Crystallinity and Optical Properties of Ag Doped ZnO Nanocomposites. *J. Compos. Sci.* **2019**, *3*, 18. DOI: 10.3390/ jcs3010018.
31. Lamba, R.; Umar, A.; Mehta, S. K.; Kansal, S. K. Sb_2O_3 ZnO Nanospindles: A Potential Material for Photocatalytic and Sensing Applications. *Ceram. Int.* **2015**, *41*, 5429 5438. DOI: 10. 1016/j.ceramint.2014.12.109.
32. Hassan Farooq, M.; Hussain, R.; Iqbal, M. Z.; Shah, M. W.; Rana, U. A.; Khan, S. U. D. Fabrication and Magnetic Properties of Sn Doped ZnO Microstructures via Hydrothermal Method. *J. Nanosci. Nanotechnol.* **2016**, *16*, 898 902. DOI: 10.1166/jnn.2016. 10705.
33. Willamson, G. K.; Hall, W. H. X Ray Line Broadening from Filed Aluminium and Wolfram. *Acta Metall.* **1953**, *1*, 22 31.
34. Khan, S. A.; Noreen, F.; Kanwal, S.; Iqbal, A.; Hussain, G. Green Synthesis of ZnO and Cu Doped ZnO Nanoparticles from Leaf Extracts of *Abutilon indicum*, *Clerodendrum infortunatum*, *Clerodendrum inerme* and Investigation of Their Biological and Photocatalytic Activities. *Mater. Sci. Eng. C* **2018**, *82*, 46 59. DOI: 10.1016/j.msec.2017.08.071.
35. He, F.; He, Z.; Xie, J.; Li, Y. IR and Raman Spectra Properties of Bi_2O_3 ZnO B_2O_3 BaO Quaternary Glass System. *AJAC.* **2014**, *05*, 1142 1150. DOI: 10.4236/ajac.2014.516121.
36. Ma, G.; Liang, X.; Li, L.; Qiao, R.; Jiang, D.; Ding, Y.; Chen, H. Cu Doped Zinc Oxide and Its Polythiophene Composites: Preparation and Antibacterial Properties. *Chemosphere* **2014**, *100*, 146 151. DOI: 10.1016/j.chemosphere.2013.11.053.
37. Sing, K. S. W.; Everett, D. H.; Haul, R. A. W.; Moscou, L.; Pierotti, R. A.; Rouquerol, J.; Siemieniewsk, T. Reporting Physisorption Data for Gas/Solid Systems With Special Reference to the Determination of Surface Area and Porosity. *Pure Appl. Chem.* **1985**, *57*, 603 619. [Database] DOI: 10.1351/ pac198557040603.
38. Xu, X. G.; Yang, H. L.; Wu, Y.; Zhang, D. L.; Wu, S. Z.; Miao, J.; Jiang, Y.; Qin, X. B.; Cao, X. Z.; Wang, B. Y. Intrinsic Room Temperature Ferromagnetism in Boron Doped ZnO. *Appl. Phys. Lett.* **2010**, *97*, 232502 232504. DOI: 10.1063/1.3524493.
39. Ju, D. X.; Xu, H. Y.; Qiu, Z. W.; Zhang, Z. C.; Xu, Q.; Zhang, J.; Wang, J. Q.; Cao, B. Q. Near Room Temperature, Fast Response, and Highly Sensitive Triethylamine Sensor Assembled with Au Loaded ZnO/SnO_2 Core Shell Nanorods on Flat Alumina Substrates. *ACS Appl. Mater. Interfaces* **2015**, *7*, 19163 19171. DOI: 10.1021/acsami.5b04904.
40. Nasir, M.; Lei, J.; Iqbal, W.; Zhang, J. Study of Synergistic Effect of Sc and C Co Doping on the Enhancement of Visible Light Photo Catalytic Activity of TiO_2. *Appl. Surf. Sci.* **2016**, *364*, 446 454. DOI: 10.1016/j.apsusc.2015.12.166.
41. Yu, W.; Zhang, J.; Peng, T. New Insight into the Enhanced Photocatalytic Activity of N , C and S Doped ZnO Photocatalysts. *Appl. Catal. B Environ.* **2016**, *181*, 220 227. DOI: 10.1016/j.apcatb.2015.07.031.
42. Sudrajat, H.; Babel, S.; Thushari, I.; Laohhasurayotin, K. Stability of La Dopants in $NaTaO_3$ Photocatalysts. *J. Alloys Compd.* **2019**, *775*, 1277 1285. DOI: 10.1016/j.jallcom.2018.10.237.
43. Kumar, S.; Sharma, V.; Bhattacharyya, K.; Krishnan, V. Synergetic Effect of MoS_2 RGO Doping to Enhance the Photocatalytic Performance of ZnO Nanoparticles. *New J. Chem.* **2016**, *40*, 5185 5197. DOI: 10.1039/C5NJ03595C.
44. Truc, N. T. T.; Duc, D. S.; Thuan, D. V.; Tahtamouni, T. A.; Pham, T. D.; Hanh, N. T.; Tran, D. T.; Nguyen, M. V.; Dang, N. M.; Chi, N. T. P. L.; Nguyen Van, N. The Advanced Photocatalytic Degradation of Atrazine by Direct z Scheme Cu Doped ZnO/g C_3N_4. *Appl. Surf. Sci.* **2019**, *489*, 875 882. DOI: 10.1016/j.apsusc.2019.05.360.
45. Molla, M. A. I.; Furukawa, M.; Tateishi, I.; Katsumata, H.; Suzuki, T.; Kaneco, S. Photocatalytic Decolorization of Dye with Self Dye Sensitization under Fluorescent Light Irradiation. *ChemEngineering* **2017**, *1*, 8. DOI: 10.3390/ chemengineering1020008.